Energy levels and Coulomb matrix elements in doped GaAs-(GaAl)As multiple-quantum-well heterostructures

Guy Fishman*
Bell Laboratories, Holmdel, New Jersey 07733
(Received 17 September 1982)

We present a simple model for calculating energy levels and envelope functions of electrons in the conduction subbands of doped GaAs-(GaAl)As multiple-quantum-well heterostructures. The model, which has no adjustable parameters, takes into account the discontinuity of the conduction-band edges at the GaAs-(GaAl)As interface and the electrostatic potential in the GaAs wells. Calculated intersubband splittings and Coulomb matrix elements are in full agreement with parameters derived from light-scattering experiments.

I. INTRODUCTION

In semiconductors the studies on a quasi-two-dimensional electron system were limited at first to inversion layers[1–3] and were subsquently extended to multiple-quantum-well heterostructures[4–7] (MQW), which are the subject of this paper. The first approach was to consider the electron motion in the plane of the layer, assumed to be infinitely thin. Such an idea was used by Stern[1] to calculate, for example, the screening length and the plasma frequency in the plane of the layer. Owing to the finite thickness of the slab (typically hundreds of angstroms in a square well of MQW), the energy levels of the electrons are quantized. The splitting between the ground level $i=0$ and the nearest subband $i=1$ is of the order of 10 meV in a typical MQW. Because of the finite thickness, the polarization effect perpendicular to the slab must be taken into account when an electron is excited from one subband to another.

This polarization field effect was discovered by Chen, Chen, and Burstein.[8] A more specific calculation was given by Allen, Jr., Tsui, and Vinter[9] and generalized by Dahl and Sham[10] to collective modes. From an experimental point of view, resonant inelastic light scattering was proposed[11,12] to study the elementary excitations of two-dimensional electron systems, and polarized (light) spectra to study the single-particle and collective excitations. The single-particle excitations have an energy which is simply the intersubband splitting $E_{ij}=E_j-E_i$; while the collective modes have an excitation energy which depends on E_{ij} and also on an effective plasma frequency. Both of them can be deduced from experiments.[13] It is then straightforward to determine the Coulomb matrix elements (CME) as defined in Refs. 9 and 10. (We shall come back briefly to this point at the end of Sec. VI.) Indeed, in polar semiconductors the collective excitations are strongly mixed with LO phonons and the existence of this coupling is the characteristic signature of the macroscopic polarization effect, as shown by Pinczuk *et al.*[13,14]

The goal of this paper is to calculate explicitly the CME.[9,10] This will permit a direct comparison between experimental data, given in Refs. 13 and 14, according to the ideas developed by Burstein *et al.*[11,12] and the theories given in Refs. 8–10.

In all experiments of interest here[13,14] it is quite reasonable, as shown below, to deal with the single-square-well model and not with the full MQW structure. In particular, our results support the analysis of Ref. 13, which uses the single-layer approximation to obtain the CME from experimental data. All the samples are n type (more precisely modulation doped[15]; i.e., with no donors in the GaAs). There is no electrical neutrality in the individual layers and the finite-electron concentration in the well leads to a band bending,[15,16] which causes changes in the energies and the wave functions of the quantified levels. Usually in a square well of a modulation-doped sample there are between $N=10^{11}$ and $N=10^{12}$ electrons per square centimeter. In the effective-mass approximation the electron wave function is a simple product of a plane wave in the plane perpendicular to the axis z of the MQW heterostructure and an envelope function $\zeta_i(z)$, where i indexes the different conduction subbands $i=0,1,2,\ldots$. Since the relevant information is contained in $\zeta_i(z)$ we shall concentrate our attention on these functions.

Contrary to the case of an inversion layer, the MQW have a mirror symmetry with respect to the plane in the middle of a square well so that the functions of an infinite-square well $\zeta_i^{(\infty)}$ or even of a finite-square well ξ_i^f, which are well known,[17] are very easy to handle. However, due to the band

bending the true envelope functions ζ_i are more difficult to calculate. If the Fermi level is between the first level $i=0$ and the second level $i=1$ (we keep the usual notations for level index) the Poisson equation relates the potential and the wave function ζ_0. If the electron concentration N is larger than a critical value N^*, the Fermi level is between the second level ($i=1$) and the third level ($i=2$) and $N=N_0+N_1$ where N_0 and N_1 are, respectively, the charge density in the levels $i=0$ and $i=1$. In this case the local charge density is proportional to $N_0\zeta_0^2+N_1\zeta_1^2$, and the calculation of the functions ζ_i is more complicated.

We calculate the functions ζ_i as a function of N (smaller or larger than N^*), because they are necessary for an evaluation of the CME. Previous papers[16] have dealt with complex calculations to be carried out on a computer. We have taken exactly the opposite point of view and we have written explicitly our intermediate results so that they can be applied to other cases without difficulties. We have, therefore, attempted a compromise between fully self-consistent, but lengthy, calculations and some crude approximations (for example, the infinite-square well). We obtain results which are in agreement with the experiments to better than 10% and which give some physical interpretation from a qualitative point of view. It is, in principle, possible to improve our results, but it should be noted that some parameters of the MQW are not always defined with an accuracy much better than 10%.[18,19] Consequently, the effort needed for the refinement of our tractable calculation seems unnecessary to us.

Finally, calculations are made at 0 K. This is quite reasonable because the experiments with which our results will be compared were performed at a liquid-helium temperature on samples with charge density N larger than 4×10^{11} cm^{-2}. In such circumstances k_BT (k_B is Boltzmann's constant; T, the absolute temperature) is less than 0.7 meV while the Fermi level is typically of the order of 15 meV.

The outline of this paper is as follows: In Sec. II we define the notation used throughout this paper and we set the conditions which justify the single-square-well model. In Sec. III we calculate the envelope functions, taking into account the band bending. In Sec. IV we introduce the definitions of the CME. We calculate the CME corresponding to $i=0\rightarrow i=1$ transitions in Sec. V and to $i=0\rightarrow i=2$ transitions in Sec. VI. We give our conclusions in Sec. VII.

In the Appendixes we have given (i) the justification of approximations used in this paper (Appendixes A and D); (ii) the calculation of the matrix elements needed to obtain the eigenenergies when the band bending is taken into account (Appendix B), and (iii) the calculation and more particularly the discussion of the different approximations of the CME (in infinite-or finite-square well, without and with band bending) (Appendix C).

II. ENVELOPE FUNCTIONS $\zeta_i^f(z)$ AND SINGLE-SQUARE-WELL MODEL

Let us begin to specify our notations. The Hamiltonian of interest here is the Hamiltonian in one dimension (z direction) of a free particle of effective mass m^* in a square-well potential (in GaAs $m^*=0.068m_0$, whose m_0 is the free-electron mass). V_w and d_1 are, respectively, the depth and the width of the square well. The center of the square well is taken as the origin and as usual the potential is zero inside the square well ($|z|<d_1/2$) and V_w outside ($|z|>d_1/2$). If the depth V_w is infinite the Hamiltonian (noted $H^{(\infty)}$) has a background state (indexed 0) energy of which is $E_0^{(\infty)}=(\pi^2/2)(\hbar^2/m^*d_1^2)$, where $2\pi\hbar$ is Planck's constant. (In the following we always use ∞ as a superscript to indicate a quantity calculated in the infinite-square well.) The eigenenergies of $H^{(\infty)}$ are $E_i^{(\infty)}=(a_i^{(\infty)})^2E_0^{(\infty)}$, with $a_i^{(\infty)}=i+1$ ($i=0,1,2,\ldots$), and the eigenfunctions are $\zeta_i^{(\infty)}$, which are sine or cosine. If the depth V_w is finite the Hamiltonian H^f has eigenenergies $E_i^f=a_i^2E_0^{(\infty)}$, where a_i is the solution[17] of

$$[(\pi/2)^2V_w/E_0^{(\infty)}-(a_i\pi/2)]^{1/2}=\begin{cases}(a_i\pi/2)\tan(a_i\pi/2) & \text{for } i \text{ even}\\ (-a_i\pi/2)\cot a_i\pi/2 & \text{for } i \text{ odd}\,.\end{cases} \tag{1}$$

If we set $b_i=(1/\pi)[E_0^{(\infty)}/(V_w-E_i)]^{1/2}$, the eigenfunctions $\zeta_i^f(z)$ of the Hamiltonian H^f can be written as

$$\zeta_i^f(z)=(2/d_i)^{1/2}n_i\times\begin{cases}\cos(a_i\pi/2)e^{1/2b_i}e^{z/b_id_1}, & z\le -d_1/2\\ \cos(a_i\pi z/d_1), & |z|\le d_1/2\\ \cos(a_i\pi/2)e^{1/2b_i}e^{-z/b_id_1}, & z\ge d_1/2\end{cases} \tag{2}$$

for i even, and

$$\zeta_i^f(z)=(2/d_1)^{1/2}n_i\times\begin{cases}-\sin(a_i\pi/2)e^{1/2b_i}e^{z/b_id_1}, & z\le -d_1/2\\ \sin(a_i\pi z/d_1), & |z|\le d_1/2\\ \sin(a_i\pi/2)e^{1/2b_i}e^{-z/b_id_1}, & z\ge d_1/2\end{cases} \tag{3}$$

for i odd. The normalization coefficient is

$$n_i=\left[1\pm\frac{\sin(a_i\pi)}{a_i\pi}+b_i[1\pm\cos(a_i\pi)]\right]^{-1/2}, \tag{4}$$

where the upper (lower) sign corresponds to i even (i odd).

Two quantities are of peculiar interest: First, the product b_id_1, which is the decay length of the $\zeta_i^f(z)$ functions outside the square well; second,

$$P_i^f=\int_{-\infty}^{-d_1/2}[\zeta_i^f(z)]^2dz+\int_{d_1/2}^{\infty}[\zeta_i^f(z)]^2dz\ , \tag{5}$$

which gives the probability of finding one electron outside the square well. All these quantities are given in Table I (there are only four bound states in all the finite-square wells of interest here) and we can now justify the single-square-well model. The distance between two square wells of width d_1 is equal to d_2+2d_3, d_2 is the thickness of the $Ga_{1-x}Al_xAs$ layer containing the donors, and d_3 is the thickness of the undoped part (see Fig. 1). For the sample where $d_1=204$ Å, $V_w=190$ meV, $d_2=200$ Å, and $d_3=0$, the decay length of $i=3$ and $i=2$ are, respectively, such that $e^{-d_2/b_id_1}=3\times10^{-3}$ and 2×10^{-4}. For the samples corresponding to $d_1=250$ Å, $V_w=120$ meV (see some other details in the following sections and in Ref. 20) $d_2=300$ Å, and $d_3=50$, 100, or 150 Å for the three samples studied. In the worst case ($d_3=50$ Å) $e^{-(d_2+2d_3)/b_id_1}=2\times10^{-4}$ for $i=3$ and 1×10^{-6} for $i=2$. We show in the following that a basis made up by the four functions ζ_i^f ($i=0,1,2,3$) is enough to calculate all the quantities of interest. The connection between two consecutive GaAs square wells is very small due to the weakness of $e^{-(d_2+2d_3)/b_id_1}$. Furthermore, we shall see that the function ζ_3^f, where b_id_1 is the largest one, plays a weak role in the calculation of CME of interest for the sample $d_1=204$ Å and no role at all for the samples $d_1=250$ Å. All this means the single-square-well model is well justified for the calculations carried out in this paper.

III. SINGLE-BAND POTENTIAL AND PERTURBED FUNCTIONS $\zeta_i(z)$

In this section we deal with the case where N is small enough ($N<N^*$) so that only the first level is occupied: The potential is given by the Poisson equation

$$\frac{d^2V}{dz^2}=\frac{4\pi e^2}{\epsilon}N\rho_0(z)\ , \tag{6}$$

where ϵ is the dielectric constant of GaAs [we sup-

TABLE I. Energies and wave functions of a square well in GaAs. First row $E_i^{(\infty)}$ gives the energies level in an infinite-square well, where $a_i^{(\infty)}=i+1$, $b_i^{(\infty)}=0$, $n_i^{(\infty)}=1$, and $P_i^{(\infty)}=0$. The other rows correspond to the finite-square wells. a_i define the cosine or sine part of the envelope functions in the square well, the product b_id_1 is the decay length outside the square well, n_i is the normalization coefficient, and P_i^f the probability of finding an electron outside of the square well. All these quantities are defined precisely in the text.

i	$E_i^{(\infty)}$ (meV)	E_i^f (meV)	a_i	b_i	n_i	P_i^f (%)	b_id_1(Å)
			$d_1=204$ Å	$V_w=190$ meV			
0	13.2	9.7	0.855	0.086	0.924	0.75	17.6
1	52.8	38.3	1.70	0.094	0.918	3.2	19.2
2	118.8	84.8	2.53	0.113	0.903	8.2	23.0
3	211.2	145.6	3.32	0.174	0.862	19.7	35.4
			$d_1=250$ Å	$V_w=120$ meV			
0	8.8	6.4	0.852	0.088	0.921	0.80	22.1
1	35.1	25.3	1.70	0.097	0.915	3.4	24.2
2	79.0	55.9	2.52	0.118	0.900	8.9	29.4
3	140.5	95.5	3.30	0.191	0.851	22.0	47.7

pose the dielectric constant of (GaAl)As is the same] and $N\rho_0(z)$ the carrier density at z. We make the simplifying assumption that

$$\rho_0(z)\approx[\zeta_0^f(z)]^2 , \tag{7}$$

which is justified because the potential V is not very sensitive to the exact form of $\rho_0(z)$; see the discussion in Appendix A.

With the use of the approximation defined by Eq. (7) the potential is given by

$$V(z)=n_0^2(4\pi e^2/\epsilon)Nd_1\begin{cases}-b_0^2[1+\cos(a_0\pi)/4]e^{1/2b_0}e^{z/b_0d_1}-K_1z/d_1+K_2, & z\le -d_1/2\\ \frac{1}{8}-\cos(a_0\pi)/4a_0^2\pi^2-\frac{1}{2}(z/d_1)^2+\cos(2a_0\pi z/d_1)/4a_0^2\pi^2, & |z|\le d_1/2\\ -b_0^2[1+\cos(a_0\pi)/4]e^{1/2b_0}e^{-z/b_0d_1}+K_1z/d_1+K_2, & z\ge d_1/2\end{cases}$$

with

$$K_1=-\frac{1}{2}-\frac{\sin(a_0\pi)}{2a_0\pi}-b_0\frac{1+\cos(a_0\pi)}{2} ,$$
$$K_2=b_0^2\frac{1+\cos(a_0\pi)}{4}-\frac{1}{2}K_1 , \tag{8}$$

where the constants are such that $V(\pm d_1/2)=0$ and V and dV/dz are continuous. This potential is consistent with the single-square-well model. If we had to take into account more than one square well we would have to modify the potential to make it periodic in the z direction.

The band binding U is defined as $V(0)-V(\pm d_1/2)$, so that

$$U\equiv V(0)-V\left(\pm\frac{d_1}{2}\right)=V(0)$$
$$=n_0^2\frac{4\pi e^2}{\epsilon}Nd_1\left[\frac{1}{8}+\frac{1}{4a_0^2\pi^2}[1-\cos(a_0\pi)]\right]$$

and is equal to 16 meV in the sample ($d_1=204$ Å, $V_w=190$ meV, and $N=4.2\times10^{11}$ cm^{-2}). The band bending U is directly proportional to d_1: For a given charge density N, the larger the width d_1, the larger the band bending U.

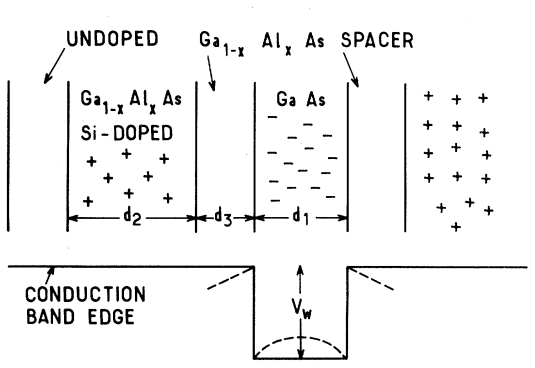

FIG. 1. Sequence of layers in modulation-doped GaAs-(GaAl)As multiple-quantum-well heterostructures. The structure of the conduction-band edge is also indicated. The dotted line shows the band bending.

Now we must find the eigenenergies and the eigenstates of the Hamiltonian $H^f+V(z)$, where H^f is the Hamiltonian of the finite-square-well solutions, which were given in Sec. II (energies, E_i^f, wave functions, ζ_i^f) and $V(z)$ is the potential defined by Eq. (8). Inside the basis made up by the four bound states $|\zeta_0^f\rangle$, $|\zeta_2^f\rangle$, $|\zeta_1^f\rangle$, and $|\zeta_3^f\rangle$, $H_0^f+V(z)$ may be written as

$$\begin{pmatrix}E_0^f+V_{00}^f & V_{02}^f & 0 & 0\\ V_{02}^f & E_2^f+V_{22}^f & 0 & 0\\ 0 & 0 & E_1^f+V_{11}^f & V_{13}^f\\ 0 & 0 & V_{13}^f & E_3^f+V_{33}^f\end{pmatrix} , \tag{9}$$

where we write $V_{if}^f=\langle\zeta_i^f|V|\zeta_j^f\rangle$. $V_{ij}^f=V_{ji}^f$ because all the matrix elements are real. $V(z)$ has even parity so that only the matrix elements such as V_{ij}^f, where i and j have the same parity, can be different from zero. The calculation of V_{ij}^f is tedious but straightforward, and is given in Appendix B.

The eigenvalues of the matrix (9) gives the splittings E_{ij}, which must be compared with experiment. The eigenstates are written as follows:

$$\zeta_0=c_0\zeta_0^f+c_2\zeta_2^f , \tag{10}$$
$$\zeta_2=c_0\zeta_2^f-c_2\zeta_0^f , \tag{11}$$
$$\zeta_1=c_1\zeta_1^f+c_3\zeta_3^f , \tag{12}$$
$$\zeta_3=c_1\zeta_3^f-c_3\zeta_1^f , \tag{13}$$

with $c_0=c_1=1$ if $N=0$.

Indeed, the matrix (9) is a truncated matrix and could be continued by other matrix elements between the functions $\zeta_i^f(z)$ and the continuum. Being smaller for the lowest-energy levels, these matrix elements have probably a large influence on the fourth level ($i=3$) whose energy is near the value of V_w, but a weaker influence on the other ones. While Eqs. (10) and (12) are quite accurate (the continuum

being negligible), Eqs. (11) and (13) are less so, because in principle we should have taken the continuum into account especially for in Eq. (13) describing the fourth level. Indeed, to calculate the CME we shall use Eqs. (10) and (12) in Sec. IV and Eqs. (10) and (11) in Sec. V and we will not need to use the most questionable equation (13) so we shall neglect the continuum which permits one to keep the calculations tractable.

To summarize, we shall use a model where the wave functions are described in a basis made up of only the four bound states of the single-square-well model, which is quite enough to calculate the CME. It is only in the case where the exact form of ζ_3 is required that our calculation becomes much more questionable. Indeed, in Table II the calculated E_{03} is the only quantity which is not in agreement with the experimental data by better than 10%. But in this paper, ζ_3 is not required for a calculation of the CME. This means, as we have already said in the Introduction, that the single-square-well model is adequate for extracting the CME from the experimental data, and this justifies the procedure of Pinczuk *et al.*[13,14]

IV. COULOMB MATRIX ELEMENTS: DEFINITIONS

In the infinite-square well the Coulomb matrix elements are equal to[9,10]

$$L^{(\infty)}(i,j;i',j')=\int_{-d_1/2}^{d_1/2}dz\left[\left[\int_{-d_1/2}^{z}dz'\zeta_i^{(\infty)}(z')\zeta_j^{(\infty)}(z')\right]\left[\int_{-d_1/2}^{z}dz''\zeta_{i'}^{(\infty)}(z'')\zeta_{j'}^{(\infty)}(z'')\right]\right]. \tag{14}$$

This relation is very useful because it is very easy to calculate and indeed the experimental data $L^{\text{expt}}(i,j;i',j')$ have been compared with $L^{(\infty)}(i,j;i',j')$ which gives the first order of approximation to the CME.[13,14]

We wish to calculate

$$L^{f}(i,j;i',j')=\int_{-\infty}^{\infty}dz\left[\left[\int_{-\infty}^{z}dz'\zeta_i^{f}(z')\zeta_j^{f}(z')\right]\left[\int_{-\infty}^{z}dz''\zeta_{i'}^{f}(z'')\zeta_{j'}^{f}(z'')\right]\right], \tag{15}$$

where the ζ_i^f are given by Eqs. (2) and (3) and[21]

$$L(i,j;i',j')=\int_{-\infty}^{\infty}dz\left[\left[\int_{-\infty}^{z}dz'\zeta_i(z')\zeta_j(z')\right]\left[\int_{-\infty}^{z}dz''\zeta_{i'}(z'')\zeta_{j'}(z'')\right]\right], \tag{16}$$

where the ζ_i are given by Eqs. (10)—(13). The numerical values of the coefficients c_i must be calculated for a given concentration. In the following we shall calculate $L^{(\infty)}(0,1;0,1)$, $L^{f}(0,1;0,1)$, and $L(0,1;0,1)$ as well as $L^{(\infty)}(0,2;0,2)$, $L^{f}(0,2;0,2)$, and $L(0,2;0,2)$ to find the relative importance of the finite-square well and the band bending before making the comparison with the experimental data. The calculation of $L^{(\infty)}(0,1;0,1)$ and

TABLE II. This table gives the energies and the Coulomb matrix elements $L(0,1;0,1)$ for a square well of width $d_1=204$ Å. We have also given the coefficients c_i, giving the mixing of the wave functions, which are needed for the calculation of $L(0,1;0,1)$.

		$d_1=204$ Å		
V_w (meV)	∞	190	190	Experimental results
N (cm^{-2})	0	0	4.2×10^{11}	(Ref. 13)
E_3 (meV)	211.0	145.6	154.4	
E_2 (meV)	118.7	84.8	95.6	
E_1 (meV)	52.8	38.3	49.5	
E_0 (meV)	13.2	9.6	25.8	
E_{03} (meV)	197.8	136.0	128.6	106
E_{02} (meV)	105.5	75.2	69.8	63.7
E_{01} (meV)	39.6	28.7	23.7	21.7
c_0 (%)	100	100	99.8	
c_2 (%)	0	0	−7.0	
c_1 (%)	100	100	99.9	
c_3 (%)	0	0	−5.4	
$L(0,1;0,1)$ (Å)	11.5	13.5	15.1	15.0

$L^{(\infty)}(0,2;0,2)$ is straightforward and gives

$$L^{(\infty)}(0,1;0,1)=\frac{5}{9\pi^2}d_1 ,$$
$$L^{(\infty)}(0,2;0,2)=\frac{5}{32\pi^2}d_1 . \tag{17}$$

V. CALCULATION OF $L(0,1;0,1)$

We begin with

$$L(0,1;0,1)=\int_{-\infty}^{\infty}dz\left[\int_{-\infty}^{z}dz'\zeta_0(z')\zeta_1(z')\right]^2 , \tag{18}$$

which, with the use of Eqs. (10) and (12), gives

$$\begin{aligned}L(0,1;0,1)=&c_0^2c_1^2L^f(0,1;0,1)+2c_0^2c_1c_3L^f(0,1;0,3)+2c_0c_1^2c_2L^f(0,1;1,2)\\&+2c_0c_1c_2c_3[L^f(0,1;2,3)+L^f(0,3;1,2)]+c_0^2c_3^2L^f(0,3;0,3)\\&+c_1^2c_2^2L^f(1,2;1,2)+2c_0c_2c_3^2L^f(0,3;2,3)+2c_1c_2^2c_3L^f(1,2;2,3)+c_2^2c_3^2L^f(2,3;2,3) .\end{aligned} \tag{19}$$

Some examples of the expression obtained for $L^f(i,j;i',j')$ are given in Appendix B (as well as numerical values).

The experiments of interest here were performed on the sample ($d_1=204$ Å, $V_w=190$ meV, and $N=4.2\times10^{11}$ cm^{-2}).[13] In this case the Fermi level is below the second level $i=1$, and Eq. (6) is applicable.

Writing here L instead $L(0,1;0,1)$ we obtain $L^{(\infty)}=11.5$, $L^f=13.5$, and $L=15.1$ Å. The experimental result is $L^{\text{expt}}=15.0$ Å. Because the calculated energies have only an accuracy of the order of 10% we must consider the agreement obtained for L as coincidental. Nevertheless, given the uncertainty on the parameters of the samples discussed in the Introduction, this result shows we obtain an excellent approximation with our simple model.

VI. CALCULATION OF L(0,2;0,2)

$L(0,2;0,2)$ was measured on three samples with the same Al composition $x=0.12$ (which gives a square well with $V_w=120$ meV), and with the following characteristics: $d_1=245$ Å, $N=5.5\times10^{11}$ cm^{-2}; $d_1=244$ Å, $N=6.8\times10^{11}$ cm^{-2}, $d_1=250$ Å, and $N=8.8\times10^{11}$ cm^{-2}. $L(0,2;0,2)$ was, respectively, found to be 4.99, 4.95, and 5.06 Å.[14] Scaling with d_1 gives a more useful comparison, $L(0,2;0,2)/d_1=0.0200$, 0.0203, and 0.0207, which are consistent with being a constant within the experimental uncertainties. (Let us recall [Eq. (17)] that $L^{(\infty)}(0,2;0,2)/d_1=0.0158$.) The band-bending effect must increase the CME [as was the case for $L(0,1;0,1)$; see the preceding section]. However, $L(0,2;0,2)$ does not depend on the charge density N. It is precisely the goal of this section to explain why.

We shall calculate all quantities of interest as a function of the charge density N ($d_1=250$ Å, and $V_w=120$ meV). Figure 2 shows typical functions for $N=6$ which corresponds to $c_2=-0.17$ (see below). Now from Eq. (16), $L(0,2;0,2)$ is given by

$$L(0,2;0,2)=\int_{-\infty}^{\infty}dz\left[\int_{-\infty}^{z}dz'\zeta_0(z')\zeta_2(z')\right]^2 . \tag{20}$$

Because ζ_0 and ζ_2 are linear combinations of the same wave functions ζ_0^f and ζ_2^f (contrary to the case of ζ_0 and ζ_1 in Sec. V) we can write $L(0,2;0,2)$ as a function of one parameter, namely c_2. For this we use $c_0=(1-c_2^2)^{1/2}$ due to the normalization, the sign of c_0 being unambiguous because $c_0=1$ when $c_2=0$. We obtain

$$\begin{aligned}L(0,2;0,2)=&(1-2c_2^2)^2L^f(0,2;0,2)+2(1-c_2^2)^{1/2}(1-2c_2^2)[L^f(0,2;0,2)-L^f(0,2;0,0)]\\&+(1-c_2^2)^2c_2^2[L^f(0,0;0,0)+L^f(2,2;2,2)-2L^f(0,0;2,2)] .\end{aligned} \tag{21}$$

We have used the symmetry properties $L(i,j;i',j')=L(j,i;i',j')=L(i',j';i,j)$. As for all the CME the calculations are tedious but straightforward. In Fig. 3 we have plotted $L(0,2;0,2)$ as a function of c_2: This is enough to show that there is saturation for increasing c_2. Physically, this results from the fact that the overlap between ζ_0 and ζ_2 has a maximum in a given range of c_2. A discussion is

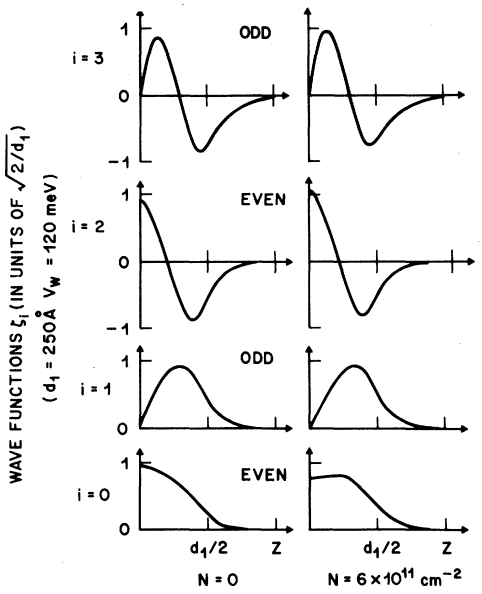

FIG. 2. This figure shows the envelope functions [more precisely $(d_1/2)^{1/2}\zeta_i$ which are dimensionless] for the square well $d_1=250$ Å, and $V_w=120$ meV. On the left-hand side is charge density $N=0$ and on the right-hand side is $N=6\times10^{11}$ cm^{-2} which gives $c_2=-17\%$ and $c_3=-13\%$.

given in Appendix C. Now we must calculate the mixing between the functions $\zeta_0(z)$ and $\zeta_2(z)$, i.e., we must calculate c_2.

In the samples where N is larger than a critical value N^*, the two first bands are occupied. $N=N_0+N_1$. In the same spirit of simplification as in Sec. II, we suppose that the potential V' is given

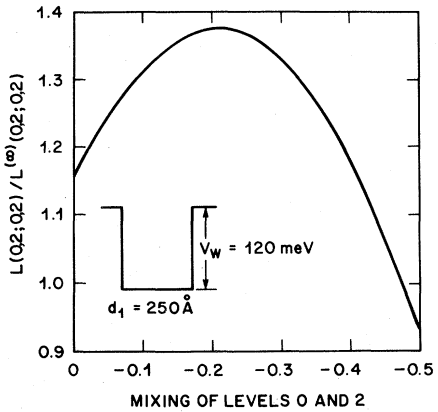

FIG. 3. This figure shows the Coulomb matrix element $L(0,2;0,2)$ as a function of coefficient c_2, defined in Eq. (10). This corresponds to the sample with $d_1=250$ Å and $V_w=120$ meV.

by

$$\frac{d^2V'}{dz^2}=\frac{4\pi e^2}{\epsilon}\{N_0[\zeta_0^2(z)]^2+N_1[\zeta_1^f(z)]^2\}\ , \quad (22)$$

where in a fully self-consistent problem ζ_0^f and ζ_1^f should be replaced by ζ_0 and ζ_1.

Even with the form given in Eq. (22) the calculations of V' can be complicated. If $N<N^*$, $N_1=0$ and the Fermi energy in level $i=0$ is merely given by

$$N_0=\frac{m^*}{\pi\hbar^2}E_F\ , \quad (23)$$

and if $N>N^*$,

$$N=N_0+N_1=\frac{m^*}{\pi\hbar^2}E_F+\frac{m^*}{\pi\hbar^2}(E_F-E_{01})$$
$$=\frac{m^*}{\pi\hbar^2}(2E_F-E_{01})\ . \quad (24)$$

if E_{01} is known, N_0 and N_1 are known. But E_{01} itself depends on the influence of the potential $V'(z)$ on the eigenstates of the finite-square well. In other words, even taking ζ_0^f and ζ_1^f instead of ζ_0 and ζ_1, we cannot avoid using a self-consistent method for calculating N_0 and N_1. However (see Appendix D), a good approximation is given by Eq. (D4) which allows us to calculate N_0 and N_1, and from Eq. (22) we obtain the potential $V'(z)$, which plays the same role, when N is larger than N^*, as the potential $V(z)$ given in Eq. (8). The potential $V'(z)$ is given in Appendix D. Under these conditions, we are able to calculate c_2 for a given charge density N and using Eq. (21), we obtain the results summarized in Fig. 4 for the energy spacings and in Fig. 5 for the CME $L(0,2;0,2)$. The overall accuracy is better than 10% and from a qualitative point of view we find again the "saturation" of $L(0,2;0,2)$: N is big enough so that the range of interest for c_2 is precisely the saturation range. This means that for $L(0,2;0,2)$ a more self-consistent calculation [ζ_i^f replaced by ζ_i in Eq. (22)] could not bring our calculated values nearer to experiment (if we stay in the same simple framework, i.e., in a basis made by the four bound states of a finite-square well).

At last we can calculate the energies of the even-parity coupled electron—LO-phonon modes corresponding to the transition E_{02}. The effect of E_{13} on the E_{02}-like modes is neglected because it has less carriers ($N_1<N_0$), it is far removed, and it is also "leaky."[14] First, we deduce the effective plasma frequency.[9,10,13]

$$E_p(0,2;0,2)=[8\pi N_0e^2L(0,2;0,2)E_{02}/\epsilon^\infty]^{1/2}\ . \quad (25)$$

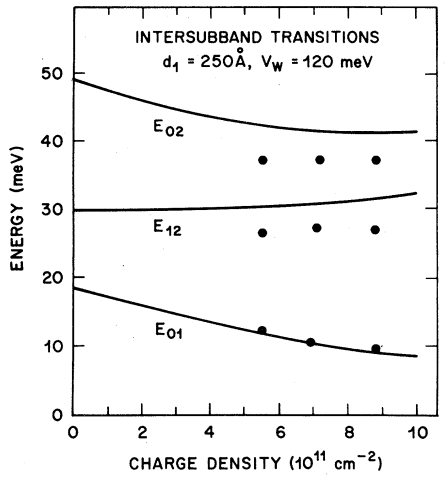

FIG. 4. Intersubband splittings as a function of the charge density N in the square well ($d_1=250$ Å and $V_w=120$ meV). The solid circles are the experimental data and the continuous lines are the theoretical curves.

Second, we deduce the coupled-mode energies $E_{\pm}^{13}$:

$$1-\frac{1}{\epsilon_L(E_{\pm})}\frac{E_p^2(0,2;0,2)}{E_{\pm}^2-E_{02}^2}=0\ , \tag{26}$$

where $\epsilon_L(E)=(E_L^2-E^2)/(E_T^2-E^2)$ accounts for the screening of the Coulomb interaction by the polar lattice. E_L (E_T) is the LO- (TO-) phonon energy in GaAs. For a given N, we have already determined N_0, E_{02}, and $L(0,2;0,2)$, so that there is *no* adjustable parameter in these calculations. Compared to the experimental data, the fact that E_{02} is too large (by about 10%) in Fig. 4 is seen again in Fig. 6, where E_+ is too large by about the same proportion.

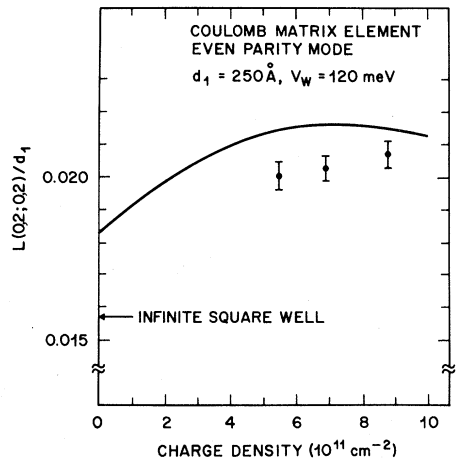

FIG. 5. Coulomb matrix element $L(0,2;0,2)$ vs the charge density N in the square well ($d_1=250$ Å and $V_w=120$ meV). The circles are the experimental data and the continuous line is the theoretical curve.

VII. CONCLUSION

It is possible to make tractable calculations in doped MQW heterostructures by means of simple approximations. Given the uncertainty in the sample parameters the calculated results are in excellent agreement with the experimental data. Adding further refinements to our calculations would be meaningful only if the overall accuracy of determinations of sample parameters could be improved.

Both the finite depth of the square well and the band bending must be taken into account in these compounds in the charge-density range of interest. The band bending increases the Coulomb matrix elements but leads to a saturation above a given value of the concentration for transition between two levels of the same parity. From a more general point of view we have shown that the single-band model used to extract the Coulomb matrix elements from the light-scattering experiments (Refs. 13 and 14) is fully justified and that the previous theories (Refs. 8–10) about the Coulomb matrix elements account well for the experimental results. In conclusion, the wave functions given in this paper are simple and reliable enough to be used elsewhere.

ACKNOWLEDGMENTS

I wish to thank A. Pinczuk and J. M. Worlock for innumerable stimulating discussions and for sug-

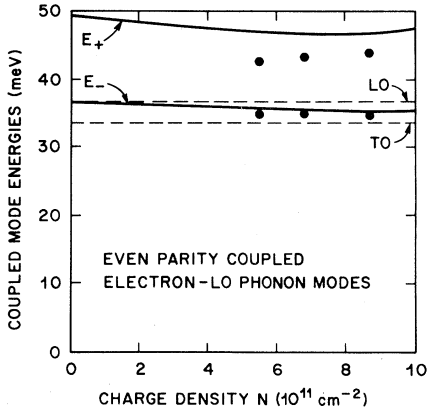

FIG. 6. Even-parity ($i=0\rightarrow i=2$) coupled electron–LO-phonon modes as a function of the charge density N in the square well $d_1=250$ Å and $V_w=120$ meV. The solid circles are the experimental data and the continuous lines are the theoretical curves. There are *no* adjustable parameters in this figure (or in any of the other figures). E_+ is larger than the experimental data mainly because the theoretical E_{02} is larger than the experimental data also (see Fig. 4).

gesting the problem. I gratefully acknowledge helpful discussions with H. L. Störmer and A. C. Gossard who supplied the necessary information about samples. I am very indebted to D. Chemla and D. A. B. Miller for a critical reading of the manuscript.

APPENDIX A

In this Appendix we justify the approximations made to calculate the potential [Eqs. (7) and (22)], i.e., to justify the use of functions ζ_i^f rather than the functions ζ_i in these equations. In the first case ($d_1=204$ Å, $V_w=120$ meV, and $N=4.2\times10^{11}$ cm^{-2}) we have calculated $|c_2|=7\%$ (Table I) and this cannot change the results significantly. In the second case ($d_1=250$ Å, $V_w=120$ meV; $0<N<10^{12}$ cm^{-2}) the problem is a little more complicated because $|c_2|$ can reach 27% for $N=10^{12}$ cm^{-2}. Up to $N\sim4\times10^{11}$ cm^{-2} the problem is the same as the preceding one and is solved in the same way. For $N>4\times10^{11}$ cm^{-2}, the Fermi level is above the bottom of the second conduction subband and the coefficient c_2 is weak but not negligible. $d^2V'/dz'\sim N_0|\zeta_0|^2+N_1|\zeta_1|^2$, and we are going to consider more specifically the first term on the right-hand side. Using Eqs. (2), (3), and (10) we obtain for the range $d_1/2<z<d_1/2$, which gives the most important contribution to the matrix elements,

$$\zeta_0^2(z)=\frac{1}{d_1}\left\{1+\cos\left[2a_0\frac{\pi z}{d_1}\right]+(c_0^2-1)\cos\left[2a_0\frac{\pi z}{d_1}\right]\right.$$
$$\left.+2c_0c_2\left[\cos\left[(a_0+a_2)\frac{\pi z}{d_1}\right]+\cos\left[(a_2-a_0)\frac{\pi z}{d_1}\right]\right]+c_2^2\cos\left[2a_2\frac{\pi z}{d_1}\right]\right\}. \tag{A1}$$

The two first terms correspond precisely to $|\zeta_0^f|^2$. The only important contribution from the other terms comes from $2c_0c_2\cos[(a_2-a_0)\pi z/d_1]$, which in the worst case ($N=10\times10^{11}$ cm^{-2}, $c_2=-27\%$) gives a term of the order of 6% of the contribution of the two first terms in the calculation of $\langle\zeta_0^f|V|\zeta_0^f\rangle$ and is completely negligible for the other diagonal terms. The contributions of $2c_0c_2\cos[(a_2-a_0)\pi z/d_1]$ to the off-diagonal terms is smaller in absolute value than the one to the diagonal terms but larger in proportion. The largest influence arises in $\langle\zeta_0^f|V|\zeta_2^f\rangle$ and is less than 20% always in the worst case ($N=10\times10^{11}$ cm^{-2}): Neglecting this term is the crudest approximation in our calculation. All the other terms in $|\zeta_0|^2$ as well as the other terms in $|\zeta_1|^2$ are negligible.

APPENDIX B

The goal of this appendix is to give the matrix elements $\langle\zeta_i^f|V|\zeta_j^f\rangle$. The functions ζ_i^f are defined in Eqs. (10)—(13) and the potential $V(z)$ in Eq. (8) via the approximation given in Eq. (7). Under these conditions, the calculations are straightforward:

$$\langle\zeta_0^f|V|\zeta_0^f\rangle=\frac{4\pi e^2Nd_1}{\epsilon}n_0^4\left[\left[\frac{1}{8}-\frac{\cos(a_0\pi)}{4a_0^2\pi^2}\right]\left[1+\frac{\sin(a_0\pi)}{a_0\pi}\right]-\frac{1}{24}-\frac{\cos(a_0\pi)}{4a_0^2\pi^2}+\frac{\sin(a_0\pi)}{4a_0^3\pi^3}\right.$$
$$-\frac{\sin(a_0\pi)}{8a_0\pi}+\frac{1}{4a_0^2\pi^2}\left[\frac{1}{2}+\frac{\sin(a_0\pi)}{a_0\pi}+\frac{\sin(2a_0\pi)}{4a_0\pi}\right]+\frac{1}{2}b_0^3\cos^4\left[\frac{a_0\pi}{2}\right]$$
$$\left.+\frac{b_0+b_0^2}{4\pi^2}K_1\cos^2\left[\frac{a_0\pi}{2}\right]+\frac{b_0K_2}{2\pi^2}\cos^2\left[\frac{a_0\pi}{2}\right]\right]. \tag{B1}$$

K_1 and K_2 are given in Eq. (8). The other diagonal terms are similar. The off-diagonal terms are a little more complicated. For example,

$$\langle \zeta_0^f \mid V \mid \zeta_2^f \rangle = \frac{4\pi e^2 N d_1}{\epsilon} n_0^3 n_2 \left\{ \left[\frac{1}{4\pi} - \frac{\cos(a_0\pi)}{2a_0^2\pi^3} \right] \left[\frac{\sin[(a_2-a_0)\pi/2]}{a_2-a_0} + \frac{\sin[(a_2+a_0)\pi/2]}{a_2+a_0} \right] \right.$$

$$- \frac{\cos[(a_2-a_0)\pi/2]}{(a_2-a_0)^2\pi} + \frac{2\sin[(a_2-a_0)\pi/2]}{(a_2-a_0)^2\pi} - \frac{\pi \sin[(a_2-a_0)\pi/2]}{4(a_2-a_0)}$$

$$- \frac{\cos[(a_2-a_0)\pi/2]}{(a_2-a_0)^2} + \frac{2\sin[(a_2+a_0)\pi/2]}{(a_2+a_0)^3\pi} - \frac{\pi \sin[(a_2+a_0)\pi/2]}{4(a_2+a_0)}$$

$$+ \frac{1}{4\pi^3 a_0^2} \left[\frac{\sin[(a_2-a_0)\pi/2]}{a_2-a_0} + \frac{\sin[(a_2+a_0)\pi/2]}{a_2+a_0} \right.$$

$$\left. + \frac{\sin[(3a_0-a_2)\pi/2]}{3a_0-a_2} + \frac{\sin[(3a_0+a_2)\pi/2]}{3a_0+a_2} \right]$$

$$+ \cos\left[\frac{a_0\pi}{2}\right] \cos\left[\frac{a_2\pi}{2}\right] \left[2\frac{b_0^4 b_2^2}{3b_2+b_0} \cos^2\left[\frac{a_0\pi}{2}\right] \right.$$

$$+ \left[\frac{1}{2\pi^2} \frac{b_0 b_2}{b_0+b_2} + \frac{1}{\pi} \frac{b_0^2 b_2^2}{(b_0+b_2)^2} \right] K_1$$

$$\left. \left. + \frac{1}{\pi^2} \frac{b_0 b_2}{b_0+b_2} K_2 \right] \right\} . \tag{B2}$$

The other off-diagonal term $\langle \zeta_1^f \mid V \mid \zeta_3^f \rangle$ is similar to this one. With $N = 4.2 \times 10^{11}$ cm^{-2}, we obtain the following with the parameters of the square well ($d_1 = 204$ Å, and $V_w = 190$ meV) given in units of meV in Table I:

$$\begin{aligned} &\langle \zeta_0^f \mid V \mid \zeta_0^f \rangle = 16.4, \quad \langle \zeta_1^f \mid V \mid \zeta_1^f \rangle = 11.5 , \\ &\langle \zeta_2^f \mid V \mid \zeta_2^f \rangle = 10.4, \quad \langle \zeta_3^f \mid V \mid \zeta_3^f \rangle = 8.5 , \\ &\langle \zeta_0^f \mid V \mid \zeta_2^f \rangle = 4.9, \quad \langle \zeta_1^f \mid V \mid \zeta_3^f \rangle = 5.6 . \end{aligned} \tag{B3}$$

From this we can calculate the energies to first order ($E_i \sim E_i^f + \langle \zeta_i^f \mid V \mid \zeta_i^f \rangle$) and compare with the energies E_i given in Table II which are exact, i.e., calculated by solving the two quadratic equations of the matrix defined in Eq. (9). The difference is small for the case $d_1 = 204$ Å, $V_w = 190$ meV, and $N = 4.2 \times 10^{11}$ cm^{-2}, but not negligible for the case $d_1 = 250$ Å, $V_w = 120$ meV, and $N > 4 \times 10^{11}$ cm^{-2}.

APPENDIX C

Here we deal with the Coulomb matrix elements. The calculation of $L^f(i,j;i',j')$ derived from Eq. (15) is straightforward. Because it is tedious, we give only two examples here:

$$L^f(0,1;0,1)=\frac{5d_1}{9\pi^2}n_0^2n_1^2\frac{9}{5\pi}\left[\frac{\pi}{2}\left[\frac{1}{(a_0+a_1)^2}+\frac{1}{(a_1-a_0)^2}\right]+\frac{\sin[(a_0+a_1)\pi]}{2(a_0+a_1)^3}+\frac{\sin[(a_0-a_1)\pi]}{2(a_1-a_0)^3}\right.$$
$$\left.+\frac{\sin(a_0\pi)}{a_0(a_1+a_0)(a_1-a_0)}+\frac{\sin(a_1\pi)}{a_1(a_1+a_0)(a_1-a_0)}\right]. \quad \text{(C1)}$$

Other terms of the form $L^f(i,j;i,j)$ are similar [let us recall that $L^{(\infty)}(0,1;0,1)=5d_1/9\pi^2$],

$$L^f(0,1;1,3)=\frac{5d_1}{9\pi^2}n_0n_1n_2n_3\frac{9}{5\pi}\left[\frac{\sin[(a_3+a_2-a_1-a_0)\pi/2]}{(a_3+a_2-a_1-a_0)(a_0+a_1)(a_2+a_3)}\right.$$
$$+\frac{\sin[(a_0+a_1+a_2+a_3)\pi/2]}{(a_0+a_1)(a_2+a_3)(a_0+a_1+a_2+a_3)}+\frac{\sin[(a_0+a_1+a_2-a_3)\pi/2]}{(a_0+a_1+a_2-a_3)(a_0+a_1)(a_3-a_2)}$$
$$+\frac{\sin[(a_0+a_1+a_3-a_2)\pi/2]}{(a_0+a_1+a_3-a_2)(a_0+a_1)(a_3-a_2)}+\frac{\sin[(a_0+a_2+a_3-a_1)\pi/2]}{(a_0+a_2+a_3-a_1)(a_2+a_3)(a_1-a_0)}$$
$$+\frac{\sin[(a_1+a_2+a_3-a_0)\pi/2]}{(a_1+a_2+a_3-a_0)(a_2+a_3)(a_1-a_0)}+\frac{\sin[(a_1+a_2-a_0-a_3)\pi/2]}{(a_1-a_0)(a_3-a_2)(a_1+a_2-a_0-a_3)}$$
$$\left.+\frac{\sin[(a_1+a_3-a_0-a_2)\pi/2]}{(a_1+a_3-a_0-a_2)(a_1-a_0)(a_3-a_2)}\right]. \quad \text{(C2)}$$

Other terms of the form $L^f(i,j;i'j')$ are similar to $L^f(0,1;2,3)$.

We give below the numerical values of $L^f(0,1;2,3)$ if the width $d_1=204$ Å. The order of $i,j;i',j'$ is the same as in Eq. (19). The unit is $L^\infty(0,1;0,1)$.

i,j,i',j'	$L^{(\infty)}(i,j,i',j')$	$L^f(i,j,i',j')$
0,1;0,1	1.000	1.172
0,1;0,3	0.100	0.124
0,1;1,2	−0.900	−1.061
0,1;2,3	0.900	1.065
0,3;1,2	0.036	0.032
0,3;0,3	0.136	0.149
1,2;1,2	0.936	1.096
0,3;2,3	0.000	−0.004
1,2;2,3	−0.900	−1.084
2,3;2,3	0.918	1.128

With $d_1=204$ Å, $L^\infty(0,1;0,1)=5d_1/9\pi^2=11.5$ Å. Without band bending, $L(0,1;0,1)=L^f(0,1;0,1)=1.172\times11.5$ Å $=13.5$ Å. With band bending and the values of coefficients c_i given in Table II, we obtain $L(0,1;0,1)=15.1$ Å. In Eq. (19) the coefficient of a term $L^f(i,j;i',j')$ is $c_ic_jc_{i'}c_{j'}$. Now why is $L^f(i,j;i',j')$ increased if we start from $L^{(\infty)}(i,j;i',j')$ and why ultimately is $L(0,1;0,1)$ larger than $L^f(0,1;0,1)$? There is no simple answer to this question. Let us look, for example, at

$$L^f(0,1;0,1)=\int_{-\infty}^{\infty}dz\left[\int_{-\infty}^{z}dz'\zeta_0^f(z')\zeta_1^f(z')\right]^2.$$

We can say that the overlap between ζ_0^f and ζ_1^f is larger than that between $\zeta_0^{(\infty)}$ and $\zeta_1^{(\infty)}$, but this must be used with some caution because this notion is not very precisely defined. [Conversely, we can say that $L^f(0,1;0,1)$ is a "measure" of the overlap between ζ_0^f and ζ_1^f.] Indeed, the most convenient way to convince oneself that the overlap between ζ_0^f and ζ_1^f is larger than the overlap between $\zeta_0^{(\infty)}$ and $\zeta_1^{(\infty)}$ is to sketch the various functions.

Another question is to ask why is $L(0,1;0,1)$ larger than $L^f(0,1;0,1)$? The answer is still more complicated: In the sum, some terms are positive and some are negative [take $L^f(0,1;1,2)$ for example]. But in this case the coefficient $c_0c_1^2c_2$ is negative too (because c_2 is negative) and gives a positive contribution. It is straightforward to analyze each term $c_ic_jc_ic_jL^f(i,j;i',j')$ and at the end one finds easily that the contribution of the positive terms is larger than the contribution of the negative terms, but we acknowledge we do not see any clear physical meaning to this result, except precisely that the "overlap" between ζ_0 and ζ_1 is larger than the overlap between ζ_0^f and ζ_1^f.

We do not give here the expressions like $L^f(0,2;0,2)$ or $L^f(0,0;0,2)$ needed to calculate $L(0,2;0,2)$ from Eq. (21) because they are tedious but straightforward. We merely say that these expressions are a little simpler than the expressions needed for the calculation of $L(0,1;0,1)$ because there are only two different coefficients $i=0,2$ in Eq. (22) instead of two, three, or four $i=0$, 1, 2, or 3 in Eq.

(19). Once again the notion of large overlap to understand why $L(0,2;0,2)$ for large N is larger than $L(0,2;0,2)$ for small N must be taken with caution. As a proof it is shown in Fig. 3 that for large N (large $|c_2|$), $L(0,2;0,2)$ is decreasing: The saturation range corresponds to the largest overlap of ζ_0 and ζ_2. In any case, from an analytical point of view, if c_0 varies from 1 to 0 ($c_0^2+c_2^2=1$) the roles of ζ_0 and ζ_2 are inverted: $[L(0,2;0,2)]_{c_0=1} \equiv [L(0,2;0,2)]_{c_0=0}$ and there is an extremum for some value of c_0 between 1 and 0. In the samples of interest, the charge density N corresponds to a maximum[22,23] (see Fig. 4).

APPENDIX D

The purpose of this Appendix is to justify Eq. (D4) used in Sec. VI to calculate N_0 and N_1. From Eq. (9) the eigenenergies E_i can be explicitly obtained (as has been done throughout this paper) but can also be written to the first order such as

$$E_{01}=E_1-E_0 \approx E_1^f-E_0^f+\langle\zeta_1^f|V|\zeta_1^f\rangle-\langle\zeta_0^f|V|\zeta_0^f\rangle \ . \tag{D1}$$

The diagonal elements $\langle\zeta_i^f|V|\zeta_i^f\rangle$ are strictly proportional to the charge density N for N smaller than the critical density N^* ($N=N_0$) and only roughly proportional to N for N larger than N^* ($N=N_0+N_1$) if N_1 is small enough by comparison to N_0. To simplify the calculations as much as possible, first we suppose this proportionality approximately holds for N larger than N^*; therefore

$$E_{01}\approx E_1^f-E_0^f+\text{const}\times N \ . \tag{D2}$$

Then we calculate E_{01} for $N=2\times10^{11}$ cm^{-2}. We obtain $E_{01}=16.2$ meV and $E_F=7$ meV. E_0^f and E_1^f are known from Table II, $d_1=250$ Å and $V_w=120$ meV. So roughly

$$E_{01}\sim 19-1.3N \ , \tag{D3}$$

where E_{01} is in meV and N in 10^{11} cm^{-2}. The relation (D3) allows us to calculate N_0 and N_1 [see Eqs. (23) and (24)], the potential used when the second level is occupied (see below), the matrix elements, and the eigenvalues of Eq. (9). The system is self-consistent if E_{01} calculated from Eq. (9) is the same as given by Eq. (D3).

Indeed, Eq. (D1) is valid as long as off-diagonal elements are negligible, i.e., as long as the charge density N is not too large. Above a given density (D1) does not hold any more and neither does (D2). Practically, we observe that for $N>7\times10^{11}$ cm^{-2}, E_{01} given by Eq. (9) is always of the order of 10 meV, which is no longer the value obtained from Eq. (D3) and which merely implies that the first-order equation (D1) is no longer valid. Eventually, we take for $0<N<10^{12}$ cm^{-2}

$$E_{01}=\begin{cases}19-1.3N, & N<7\\ 10, & 7<N<10\end{cases} \tag{D4}$$

where E_{01} is in meV and N in 10^{11} cm^{-2} and we will be satisifed if E_{01} obtained from Eq. (9) and Eq. (D4) differ by less than 1 meV, *as is indeed the case.* The results given in Fig. 5 are obtained from Eq. (9). We can, therefore, conclude that a more refined calculation could give some different values for the splittings E_{ij} but would not change anything in the range of interest ($7\times10^{11}<N<9\times10^{11}$ cm^{-2}) in making a comparison with the experimental data because this is precisely the saturation range of $L(0,2;0,2)$: In this range the precise value of $L(0,2;0,2)$ does *not* depend on the precise value of the coefficient c_2.

Finally, we give the potential $V'(z)$. For $N>N^*$, Eq. (22) gives the following potential (with $p_0=N_0/N$ and $p_1=N_1/N$):

(i) For $|z|<d_1/2$,

$$V'(z)=n_0^2\frac{4\pi e^2}{\epsilon}Nd_1\left[\frac{1}{8}\left[p_0+p_1\frac{n_1^2}{n_0^2}\right]-p_0\frac{\cos(a_0\pi)}{4a_0^2\pi^2}+p_1\frac{n_0^2}{n_1^2}\frac{\cos(a_1\pi)}{4a_1^2\pi^2}-\left[p_0+p_1\frac{n_1^2}{n_0^2}\right]\frac{1}{2}\left[\frac{z}{d_1}\right]^2 + p_0\frac{\cos(2\pi a_0 z/d_1)}{4a_0^2\pi^2}-p_1\frac{n_1^2}{n_0^2}\frac{\cos(2\pi a_1 z/d_1)}{4a_1^2\pi^2}\right],$$

(ii) for $z>d_1/2$,

$$V'(z)=n_0^2\frac{4\pi e^2}{\epsilon}Nd_1\left[-p_0b_0^2\frac{1+\cos(a_0\pi)}{4}e^{1/2b_0}e^{-z/b_0d_1}-p_1\frac{n_1^2}{n_0^2}b_1^2\frac{1-\cos(a_1\pi)}{4}e^{1/2b_1}e^{-z/b_1d_1} \pm K_1'\frac{z}{d_1}+K_2'\right],$$

where the sign before K'_a is positive if $z > d_1/2$ and negative if $z < -d_1$, with

$$K'_1 = -\frac{1}{2}\left[p_0 + p_1\frac{n_1^2}{n_0^2}\right] - p_0\left[\frac{\sin(a_0\pi)}{2a_0\pi} + b_0\frac{1+\cos(a_0\pi)}{2}\right] + p_1\frac{n_1^2}{n_0^2}\left[\frac{\sin(a_0\pi)}{2a_0\pi} + b_0\sin^2\left[a_0\frac{\pi}{2}\right]\right]$$

and

$$K'_2 = -\tfrac{1}{2}K'_1 + \tfrac{1}{2}p_0 b_0^2\cos^2\left[a_0\frac{\pi}{2}\right] + \tfrac{1}{2}p_1\frac{n_0^2}{n_1^2}\sin^2\left[a_1\frac{\pi}{2}\right].$$

It is easy to see that if $p_0 = 1$, $p_1 = 0$, and $V'(z) = V(z)$.

---

*On leave of absence from Groupe de Physique des Solides de l'Ecole Normale Supérieure, Université Paris VII, 2 place Jussieu, 75251 Paris Cedex 05, France.

[1]F. Stern, Phys. Rev. Lett. 18, 546 (1967).

[2]F. Stern and W. E Howard, Phys. Rev. 163, 816 (1967).

[3]F. Stern, Proceedings of the 2nd International Conference on Solid Surfaces, City, Japan, 1974 [J. Appl. Phys. Suppl. 2, (1974)].

[4]L. Esaki and R. Tsu, IBM, J. Res. Dev. 14, 61 (1970).

[5]L. E. Esaki, *Proceedings of the International Conference on Physics and Chemistry of Semiconductor Heterojunctions and Layer Structures, Budapest, 1970* (Akademiai Kiado, Budapest, 1971), Vol. 1, p. 13.

[6]Yu. A. Romanov, Fiz. Tekh. Poluprovodn. 5, 1434 (1971) [Sov. Phys.—Semiconductors 5, 1256 (1972)].

[7]Yu. A. Romanov and K. Orlov, Fiz. Tekh. Poluprovodn 7, 253 (1973) [Sov. Phys.—Semiconductors 7, 182 (1973)].

[8]W. P. Chen, Y. J. Chen, and E. Burstein, Surf. Sci. 58, 263 (1976).

[9]S. J. Allen, Jr., D. C. Tsui, and B. Vinter, Solid State Commun. 20, 425 (1976).

[10]D. A. Dahl and L. J. Sham, Phys. Rev. B 16, 651 (1977).

[11]E. Burstein, A. Pinczuk, and S. Buchner, in *Physics of Semiconductors 1978,* edited by B. L. H. Wilson (IOP, London, 1979), p. 1231.

[12]E. Burstein, A. Pinczuk, and D. L. Mills, Surf. Sci. 98, 451 (1980).

[13]A. Pinczuk, J. M. Worlock, H. L. Störmer, R. Dingle, W. Wiegmann, and A. C. Gossard, Solid State Commun. 36, 43 (1980).

[14]A. Pinczuk and J. M. Worlock, Surf. Sci. 113, 69 (1982) and (private communication).

[15]H. L. Störmer, Proceedings of the 15th International Conference on Physics of Semiconductors, Kyoto, 1980) [J. Phys. Soc. Jpn. 49, Suppl. A 1013 (1980)].

[16]T. Ando and S. Mori, J. Phys. Soc. Jpn. 47, 1518 (1979); 48, 865 (1980).

[17]L. I. Schiff, *Quantum Mechanics,* 3rd ed. (McGraw-Hill, New York, 1968).

[18]A. C. Gossard (private communication).

[19]R. Dingle, in *Proceedings of the 13th International Conference on the Physics of Semiconductors, Rome, 1976,* edited by F. G. Fumi (North-Holland, Amsterdam, 1976), p. 965.

[20]H. L. Störmer, A. Pinczuk, A. C. Gossard, and W. Wiegmann, Appl. Phys. Lett. 38, 691 (1981).

[21]As a matter of fact, the two approximations (single-square well; continuum neglected) are linked: It is only if the continuum can be neglected that it is possible to say that the overlap between functions of two different square wells is negligible.

[22]This relation is valid except if $i = j = i' = j' = 0$ (see Ref. 10) but we do not deal with this case.

[23]As a function of c_0 (or c_2 which has the same meaning) $L(0,2;0,2)$ has two extrema for $0 < c_0 < 1$: a maximum and a minimum. The orders of magnitude of the charge density are such that only the maximum can be reached.